Polymer surface science

A. Opdahl, S. Hoffer, Bénédicte Mailhot-Jensen, G.A. Somorjai

Polymer Surface Science

A. OPDAHL,[1,2] S. HOFFER,[1,2] B. MAILHOT,[1,2,3] G.A. SOMORJAI[1,2*]
[1]Department of Chemistry, University of California, Berkeley, California 94720
[2]Material Science Division, Lawrence Berkeley National Laboratory, Berkeley, California 94720
[3]Laboratoire de Photochimie Moléculaire et Macromoléculaire, UMR CNRS 6505, Ensemble Universitaire de Cézeaux, 63177 Aubière Cedex, France

ABSTRACT: Molecular level studies of the structure and mechanical properties of polymer surfaces have been carried out by sum frequency generation (SFG) surface vibrational spectroscopy and atomic force microscopy (AFM). The surfaces of different grades of polyethylene and polypropylene have been characterized—including during the glass transition and when mechanically stretched. Copolymers that have hard and soft segments with different glass transition temperatures show phase separation, an effect of hydrogen bonding between the hard and soft segments, that influences their adhesive and friction properties. AFM and SFG show that low surface energy additives migrate to the surface and alter the surface mechanical properties. Polymers, where the chemical nature of the end groups is different from the backbone, show surface segregation of the hydrophobic part of the chain in air and the hydrophilic part in water. Likewise, in miscible polymer blends, surface segregation of the more hydrophobic component in air and the more hydrophilic component in water is observed. This area of surface science requires increased attention because of the predominance of polymers as structural materials and as biomaterials.

Key words: polymer surfaces; force microscopy (AFM); sum frequency generation (SFG) vibrational spectroscopy

Introduction

Investigations of surfaces at the atomic and molecular levels by a large number of techniques that have become available over the last 30 years has brought the chemistry and physics of surfaces to the frontiers of these disciplines. Much of the research has focused on metal and oxide surfaces.[1] Their structure, composition, dynamics, and electrical and mechanical properties have been explored. The structure, bonding, mobility, and reactions of adsorbates on these surfaces have been elucidated. Polymer surfaces, however, have been studied to a lesser extent though their importance as structural materials and implants in biological and medical applications has been dramatically increasing.

Over the past 5 years our laboratory has been studying polymer surfaces by techniques that have been recently developed: sum frequency generation (SFG) surface vibrational spectroscopy and force microscopy (FM). This paper summarizes the results of our study, in which we used polymer surfaces such as polyethylene and polypropylene, as well as polymer blends. The structures of these polymer surfaces were monitored, as were key mechanical properties (friction coefficient and elastic modulus), to establish structure/mechanical property relationships. Changes of polymer surface composition as the interface was changed from air to water were measured. One of the unique properties of polymers is that they are mechanically flexible, which plays important roles in many of their applications. Thus, we have also studied the changes of surface structure as the polymer is stretched.

Polymer Information

The structures of all of the polymers presented in this review are shown in Figure 1. Relevant material properties are given in Table 1. High and low density polyethylene (HDPE and LDPE), isotactic, and atactic polypropylene (iPP and aPP), and polyethylene glycol (PEG) were purchased from Aldrich Chemical. The polyurethane samples and the biopolymer samples were synthesized by the Polymer Technology Group in Berkeley, CA. The commercial polyethylene sample was provided by Union Carbide.

Table 1. Material properties of the polyolefins presented in this review.

	LDPE	HDPE	aPP	iPP
Density (g/cm^3)	0.92	0.95	–	0.90
Crystallinity (%)	23	65	2	63
Elastic modulus (GPa)	0.2	1	–	–
Yield stress (MPa)	10	25	–	–
Yield strain %	10	6		
Glass temperature	~160 K	~160 K	~260 K	~260 K

Experimental Techniques

IR+Visible SFG Vibrational Spectroscopy

SFG vibrational spectroscopy is a nonlinear optical technique that probes the second order nonlinear susceptibility of a material, $\chi^{(2)}$.[2] In our applications, we use SFG to generate a vibrational spectrum of the molecules at an interface. The surface specificity arises from the fact that under the electric dipole approximation, even-ordered nonlinear processes ($\chi^{(2)}$) vanish in a centrosymmetric media. Thus, a sum-frequency signal is ob-

tained from an interface (where centrosymmetry is broken), while no signal is obtained from the centrosymmetric bulk.

The experimental setup involves overlapping a visible and a tunable infrared laser beam on a polymer surface to induce a polarization at the sum frequency ($\omega_{SUM} = \omega_{VIS} + \omega_{IR}$). The visible beam ($\omega_{VIS}$) is 532 nm light generated by frequency doubling the 1064 nm fundamental output from a Continuum YAG-PY61 laser (generating ~20 ps pulses at 20 Hz). The infrared beam (ω_{IR}), tunable from 1300 to 4000 cm^{-1}, is generated from a combined OPG/OPA [(optical parametric generation)/(optical parametric amplification)] system composed of KTP crystals pumped by the fundamental output of the YAG laser at 1064 nm. The sum-frequency output signal is collected by a gated integrator and a photon counting system.

Vibrational spectra are obtained by tuning the infrared beam and measuring the sum-frequency signal as a function of the infrared frequency. Resonant enhancement occurs at frequencies that are both IR and Raman active modes of the surface. Additionally, the sum frequency signal increases as the square of the number of molecules at the surface and is generally enhanced if those molecules are well ordered. Spectra collected using the $s_{sum}s_{vis}p_{IR}$, $s_{sum}p_{vis}s_{IR}$, and $p_{sum}p_{vis}p_{IR}$ polarization combinations probe different spatial components of ($\chi^{(2)}$) (a 27 component, rank three tensor) and can be used to determine the orientation of molecules at the interface.[3,4] The approximate area (in the plane of the surface) probed is of the order of square millimeters.

SFG has been applied to several types of chemical systems where a detailed knowledge of the chemical composition and structure of the surface layer is important. These systems include adsorbates on metal surfaces,[5,6] liquid surfaces,[7] electrochemical systems,[8] and recently, polymers. Within the field of polymer science, SFG is being used to study a variety of surface phenomena, including orientation effects on rubbed polymer films,[9] surface structural differences between crystalline and amorphous polymers,[10] surface segregation,[11] and degradation of polymer surfaces by plasma and radiation.[12] As SFG has been applied to the study of more and more types of interfaces, specific details are being addressed. Methods have been presented for determining the surface specificity of the technique and for measuring higher order contributions (quadrupole) to the sum frequency signal.[13,14] Methods have also been developed to incorporate variables like surface roughness into the description of the orientation of interfacial molecules.[15,16]

Force Microscopy

Atomic force microscopy (AFM) involves the interaction of a small probe with a surface and is used in our lab to image the microscopic features of polymer surfaces. In addition, we use the AFM to apply forces to the polymer surface in order to measure surface mechanical properties of polymers, such as friction force, elastic modulus, and hardness. A typical AFM applies loads in the nanonewton regime. We have used several other instruments that measure surface mechanical properties under higher loading conditions. The forces we have applied in our experiments range from a few nanonewtons with the AFM, to micronewtons with the diamond probe scanning force microscope (SFM), to several newtons with the classical pin-on-disk apparatus (POD).

AFM (low loads)

Several force microscopes were used in the experiments described in this paper. A commercial Park Scientific M5 AFM with a large range scanner was used to collect topographic and friction images of ~500 square micron areas and also to measure the elastic modulus and hardness of polymers in ambient conditions. Commercial silicon cantilevers with tungsten carbide coated tips from NT-MDT were used with this instrument. A homebuilt AFM using an interferometric detection scheme[17] was used to quantify the elastic modulus, friction, and hardness of polyethylene and polypropylene surfaces under minimum pressure. The cantilever for this instrument was prepared by bending a tungsten wire at a right angle and etching one end (radius of curvature ~1 micron), which was used as the tip.

A homebuilt walker-style AFM[18] that can be evacuated to 10^{-5} Torr was used to heat and cool polymer samples. The sample is stationary and can be heated or cooled without heating or cooling other components of the microscope. The deflection of the cantilever is detected by a light beam and a position sensitive photodiode. Commercial silicon cantilevers with tungsten carbide coated tips from NT-MDT were used.

SFM (intermediate loads)

Friction testing at the microscale was performed with an SFM consisting of an atomic force microscope (Digital Instruments, Nanoscope II) retrofitted with a capacitor force transducer (Hysitron, Inc.). The vertical and lateral (friction) forces were determined by two independent capacitor plates that were calibrated for each tip.[19] A three-sided pyramidal diamond tip with radius of curvature 100 nm and conical diamond tips with radius of curvature equal to 16 and 20 μm were used to scan the surfaces at loads in the range of 5–1000 μN.

POD (large loads)

A POD setup[20] was used to perform friction testing at the milliscale. A cantilever beam holding the pin was wired with four strain gauges in a Wheatstone bridge configuration. The normal force was applied directly as a dead weight, and the friction force was measured by the strain gauges. The strain gauge output voltage was passed through an amplifier before collection by a data acquisition system. Friction coefficient data were collected continuously at a rate of 1.5 Hz. A blunt, diamond coated tip with radius 1.2 mm was used.

Measurements

Friction

The frictional force was measured on the AFM by monitoring the lateral deflection of the cantilever while scanning the cantilever over the same region of the surface, from left to right and then from right to left. The difference between these two scans represents twice the frictional force. This is done because it is difficult to establish the zero of the frictional force, and to reduce the effect of topographic artifacts (surface roughness) on the friction. A friction coefficient is defined as the slope of a friction force versus applied load curve.

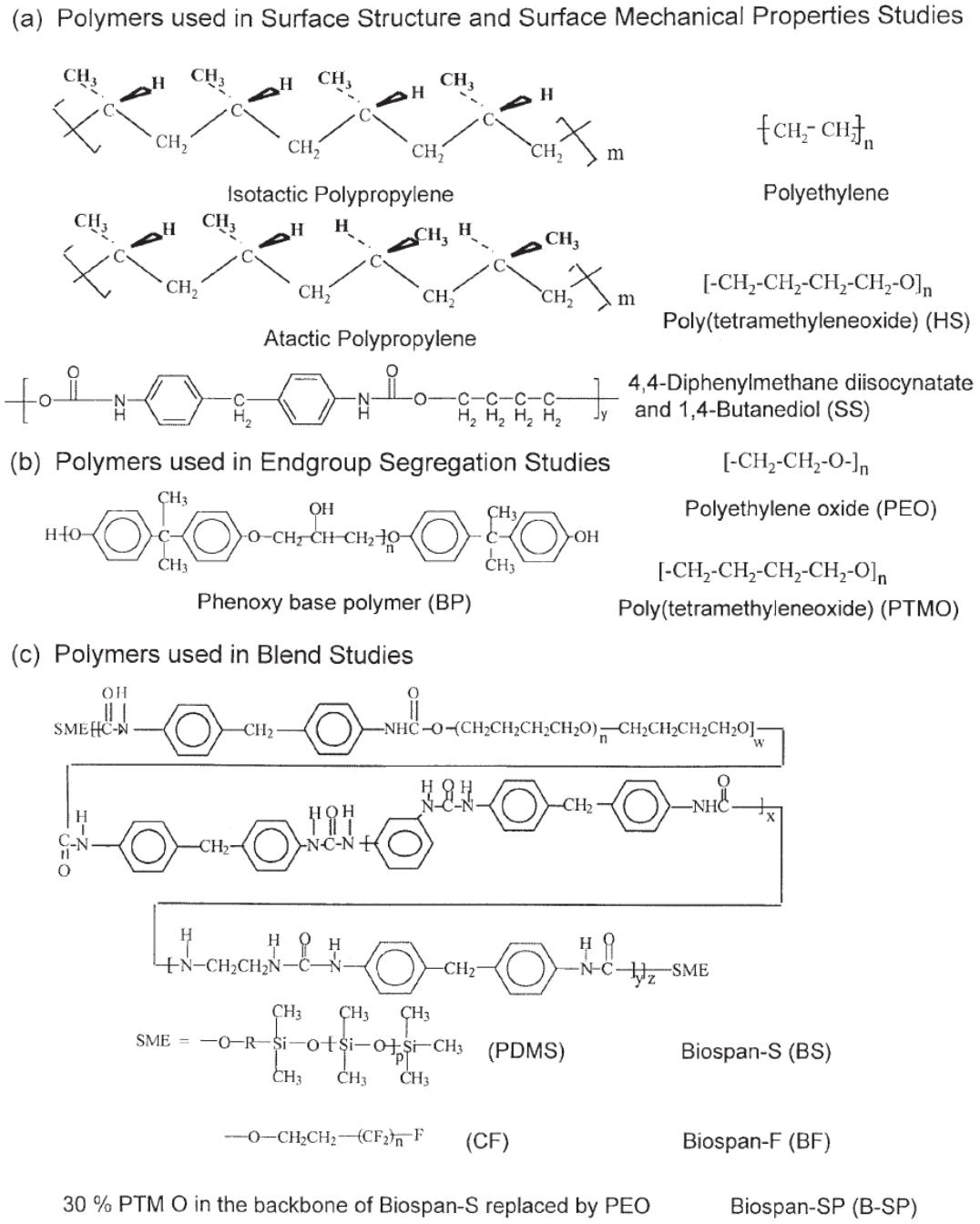

Fig. 1. Chemical structure of the polymers presented in this paper.

Elastic modulus (stiffness)

The techniques used for measuring the elasticity of the polymer surface can be found in references 21 and 22. Briefly, the elastic modulus was measured by oscillating the cantilever at an amplitude of ~1 nm and at a frequency far below its resonance frequency.[21] When the cantilever comes in contact with the sample the oscillation amplitude is damped. The extent of damping depends on the elastic modulus of the sample. The greater the amplitude of oscillation of the cantilever (in contact with the surface), the lower the elastic modulus of the sample and vice versa.

A second method used to determine the elastic modulus is through analysis of interaction force curves between the tip and the surface.[22] The interaction force curve (Fig. 2) describes the response of the cantilever as the tip is pressed into contact with the polymer surface. The distance the tip moves into the sample reflects the elasticity of the sample. The greater the elastic modulus of the surface, the lower the elastic penetration depth of the tip into the surface. This is measured as a larger slope on the repulsive part of the interaction force curve. Details of the measurement of elastic modulus and hardness using the SFM can be found in references 23 and 24.

Hardness

Hardness was measured by using the AFM tip to plastically deform the polymer surface. The tip was pushed into the surface with enough pressure to form a permanent indent. The indent was imaged later with the same tip. The hardness was defined as the indentation load divided by the area of the indent.

Results

Surface Structures of Polymers

Polyethylene

We have collected SFG spectra of several polymers including polyethylene (PE) and polypropylene (PP), which represent

chemically simple polymer systems composed of only carbon and hydrogen. The grades of PE and PP exhibit different degrees of crystallinity depending on chain length, chain branching ratio, and tacticity. Both PE and PP have similar surface energies and have glass temperatures that are below room temperature (~160 K for PE and ~260 K for PP). Our measurements at room temperature represent measurements of semicrystalline polymers with the amorphous phase in the rubbery state.

We have used SFG to study the effect of crystallinity on PE surface structure by collecting spectra of LDPE and ultra high molecular weight polyethylene (UHMWPE). The SFG spectra of these two polymers are shown in Figure 3 and are markedly different, indicating that they have different surface structures. For LDPE, the band at 2850 cm^{-1} is attributed to the CH_2 symmetric stretch, and the band at 2826 cm^{-1} is attributed to the CH_2 antisymmetric stretch. For UHMWPE, both of these bands are shifted to higher frequencies. This blue shift indicates that there are more gauche conformers at the polymer surface.[25,26] Gauche conformers are consistent with the chain folded lamellar structure of UHMWPE shown in the inset of Figure 3. In the case of LDPE, a highly branched and more loosely organized grade of PE, the peak at 2850cm^{-1} indicates that mostly trans conformers exist at the surface. The random packing of the LDPE surface is evidenced by the larger bandwidths of the SFG peaks.

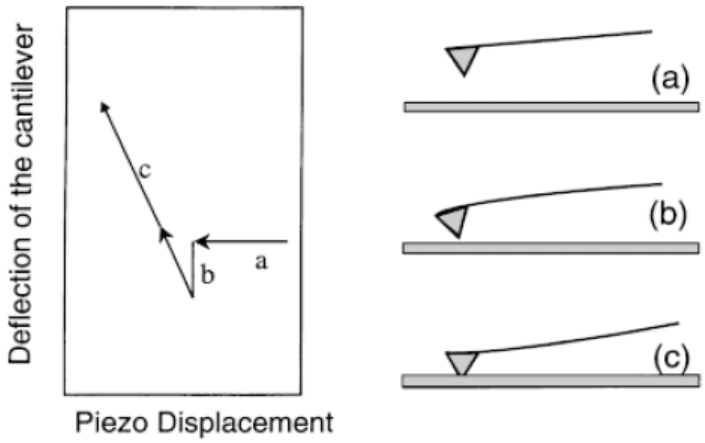

Fig. 2. AFM interaction force versus distance curve showing (a) tip far from sample (b) tip snap into contact with sample, and (c) increasing load and pressing into sample.

Polypropylene

SFG spectra of aPP and iPP, two structural isomers of polypropylene, are shown in Figure 4. They are quite different from one another, indicating a difference in surface structure. aPP has individual monomers that are arranged in a steriochemically random fashion, whereas iPP is stereochemically regular and is highly crystalline (>60%). The SFG spectra of aPP shows a small CH_2 symmetric peak at 2845 cm^{-1} relative to the CH_3 symmetric peak at 2883 cm^{-1}. In contrast, the CH_2 symmetric

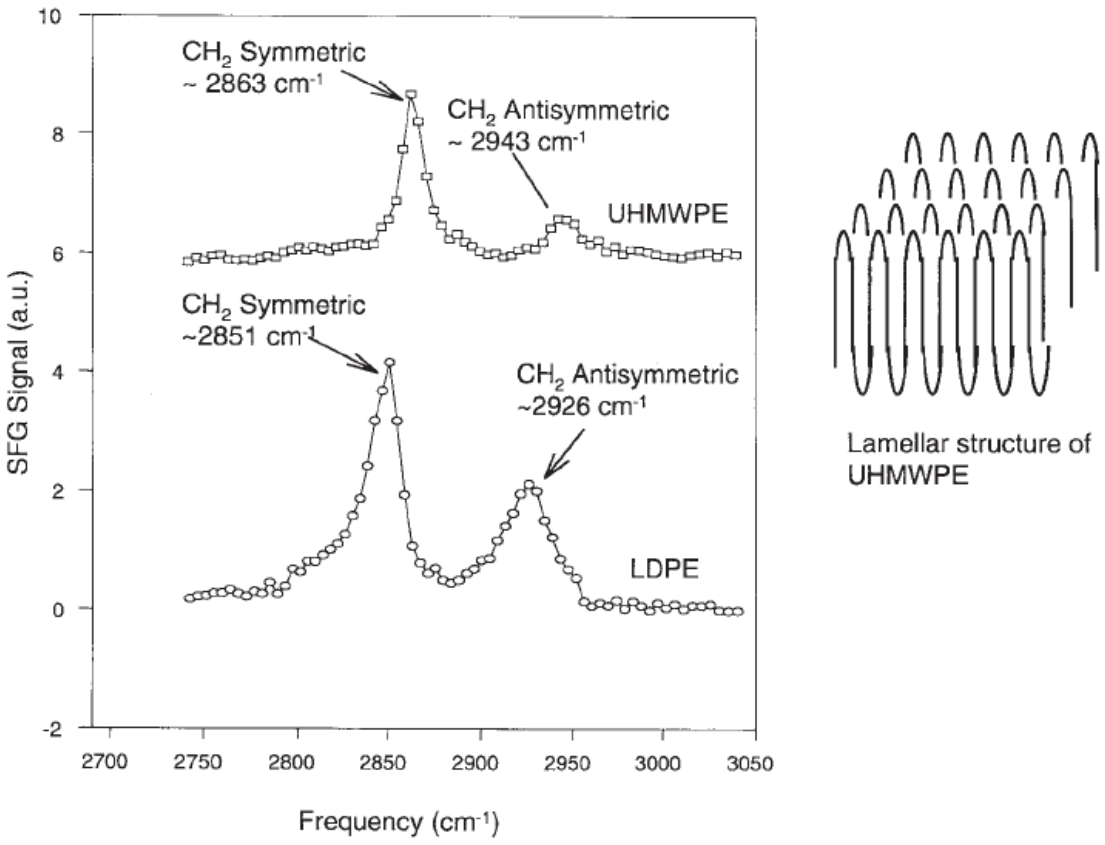

Fig. 3. SFG spectra of LDPE and UHMWPE (ssp polarization). Inset: lamellar structure of UHMWPE.

peak is much larger compared to the CH_3 symmetric stretch for the iPP surface. This indicates that the backbone of aPP is relatively randomly oriented at the surface and that the pendant methyl groups point away from the surface. For iPP, crystallinity imposes an order to the surface. Crystalline iPP chains are generally helical with the pendant methyl groups staggered by 120°.[27] The SFG results are consistent with this crystalline state where a fraction of the CH_2 groups are constrained to point away from the surface.

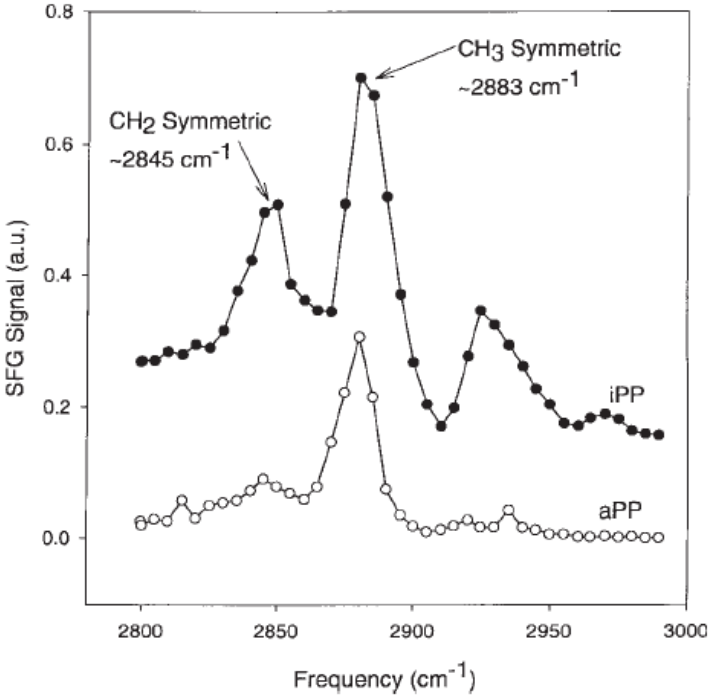

Fig. 4. SFG spectra of aPP and iPP (ssp).

Changes in the Polypropylene Surface Structure at the Glass Transition

Temperature has a strong effect on the surface structure and mechanical properties of polymers. An example is the transition from a rubbery to a glassy state—the glass transition.[28] Mechanically, the amorphous component of the polymer undergoes a transition from a rubbery state above the transition temperature to an elastically rigid glassy state below it. This is measured as a large increase in the elastic modulus of the polymer as the polymer is cooled.

A number of investigators are using AFM to study the glass transition of thin polymer films.[29,30,31] In particular, to determine how the free interface (air-polymer interface) and film thickness affect the glass temperature of the film's surface. It has been suggested that enhanced free volume (leading to enhanced mobility) at the surface of a polymer gives the surface a lower glass temperature than the polymer bulk.[29] It has also been suggested that hydrostatic pressure generated beneath the AFM tip can increase the glass temperature of the surface. Recent efforts have demonstrated that the dynamic nature of the AFM measurement plays a significant role in determining the apparent glass temperature.[30,31]

In our lab, we have used SFG and AFM to measure the structural changes that are associated with the mechanical property changes at the glass transition.[32] AFM interaction force curves were measured on aPP and iPP surfaces as a function of temperature in vacuum pressures of 10^{-5} Torr. The slope of the approach curve was used as a signature of modulus changes in this temperature regime. For the same cantilever, the higher

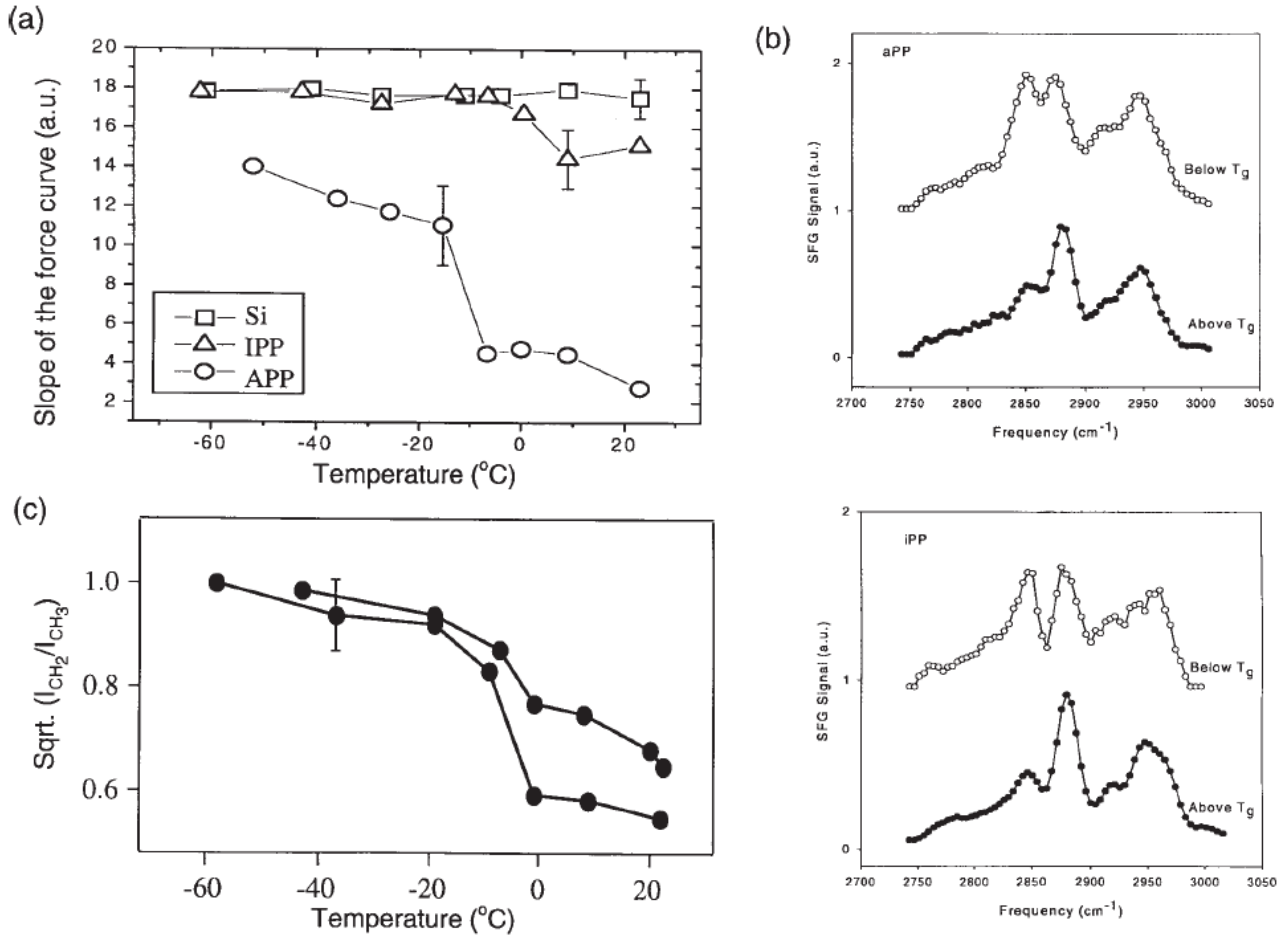

Fig. 5. (a) Slope of AFM approach curve versus temperature. (b) SFG spectra of aPP and iPP above and below the glass temperature (ssp). (c) Square root of I_{CH_2}/I_{CH_3} as a function of temperature.

the slope of the curve, the greater the elastic modulus. From several temperature runs, the representative changes observed for iPP, aPP, and a silicon wafer (used as a reference) are plotted in Figure 5(a). For both iPP and aPP, there is an increase in the surface elastic modulus at temperatures below the glass temperature. For aPP, a rapid change of the modulus occurs between 0 and –20°C. For iPP, the change is smaller and occurs around 0°C.

SFG spectra were collected as a function of temperature in vacuum pressures of 10^{-5} Torr. Figure 5(b) shows SFG spectra for aPP and iPP above and below the glass transition. An increase in the ratio of the symmetric stretch of the CH_2 group to the CH_3 group in both aPP and iPP was observed on cooling through the glass transition.

The ratio of the strengths of these two modes is plotted to qualitatively describe how the surface structure changes with temperature [Fig. 5(c)]. The data show that the ratio has a sharp increase in the temperature range between 0 and –20°C and is more prominent for aPP than iPP. Because the bulk glass transition of polypropylene occurs in this temperature region, the observed spectral change is directly correlated to the glass transition.

This spectral change across T_g indicates that the CH_2 groups become better polar-oriented below T_g. In polypropylene the CH_2 groups form the backbone of the polymer chain and the CH_3 groups are the side (pendant) groups. Our observation suggests that below T_g, the polymer backbone becomes more ordered and controls the surface structure—the CH_2 groups point out of the surface. Above T_g, the polymer backbone is more disordered. The CH_2 groups are more randomly oriented, which results in a decreased CH_2 peak intensity. The CH_3 groups, being more hydrophobic, orient preferentially away from the surface.

The temperature dependence of the SFG and AFM results for aPP and iPP show that the enhanced ordering of the backbone (polymer chains) correlates to the increased surface modulus. Both are induced by the transition to the glass phase. The more prominent spectral change for aPP compared to iPP in both SFG and SFM measurements confirms that the changes are associated with the glass transition of the polymer.

Surface Mechanical Properties

In addition to measuring the polymer mechanical properties as a function of temperature, we have measured in detail the elastic modulus and friction properties as a function of pressure. Pressure is an extremely important concept in the mechanical testing of polymers. Semicrystalline polymers, like polyethylene and polypropylene, behave elastically when small pressures and strains are applied.[33,34] As higher strains and pressures that exceed the yield strain and yield stress of the polymer are applied, the polymer will behave plastically and in some cases will strain soften.

When an AFM tip or other indentor applies stress to a polymer surface the response of the polymer can be very complex and will depend on the relationship of the polymer elastic modulus and yield stress to the contact pressure. The amount of time that stress is applied is also a critical factor—most polymers exhibit time-dependent relaxation processes. Finally, depending on the microstructure of the polymer, probing different sized contact areas (with different sized indentors) may lead to completely different responses of the polymer. All of these effects can be observed by monitoring the elastic modulus and friction properties with the AFM.

At the most basic level, Hertzian contact mechanics defines the mean pressure between a spherical indentor (like an AFM tip) and an elastic surface by Equation 1. W is the applied load, E is the elastic modulus of the polymer, ν is the Poisson ratio of the polymer, and R is the radius of curvature of the indentor.[35]

$$P = \frac{2}{3}\left(\frac{6WE^2}{\pi^3 R^2 (1-\nu)^2}\right)^{1/3} \quad (1)$$

Pressure can be reduced by either decreasing the applied load or by increasing the radius of curvature of the indentor. Our lowest pressure experiments were performed with the AFM using tips of large radii of curvature (1 micron).[21] These measurements (applying loads of 1–1000 nN) are highly surface sensitive and probe the top 0.1 to 10 nm of the surface. They also probe larger contact areas (10^{-4}–10^{-2} square microns) as compared to those done with typical commercial AFM tips (radii ~20 nm). All three of the instruments described earlier (AFM, SFM, and POD) are capable of applying high pressure to the polymer surface. The POD apparatus applies that pressure to the largest area.

Mechanical properties under low contact pressure

At low pressure, the penetration of the indentor into the polymer surface is minimal and the deformation of the polymer is largely elastic—the properties measured will closest reflect the true elastic properties of the surface. We have carried out low pressure and low penetration depth experiments using the AFM and blunt tips (radius of curvature ~1000 nm).

This approach has been used to monitor the elastic modulus, hardness, and friction of a series of polyolefins: LDPE, HDPE, iPP, and aPP in the load range of 10^{-8}–10^{-6} N and in the 1–150 MPa pressure range. Figures 6 and 7 show the effects of pressure on elastic modulus and friction. Comparing the four polymers, the expected trend of increased elastic modulus with increased density and crystallinity is seen (Table 1). Additionally, for each polymer, the elastic modulus increases linearly with contact pressure. The linear increase is strong for LDPE, HDPE, and iPP but less so for aPP, which has a very low yield stress (2 MPa). The low yield stress of aPP indicates that even under the low contact pressures in this experiment, the tip plastically damages the surface. For the other three polymers, the applied pressure is relatively low, and the linear increase of the elastic modulus with pressure is associated with primarily elastic deformation of the polymer.

The friction process for all four polymers is dominated by the deformation (elastic and plastic) of the polymer surface. The highest friction coefficient was observed on the aPP surface. Again, this is attributed to the low yield stress of aPP, which leads to plastic wear of the surface. For the other three polymers, within the elastic loading regime, friction versus load curves show characteristics predicted by the JKR model of contact area. The JKR model incorporates adhesive effects in the tip interaction and describes such phenomenon as friction at negative loads (i.e., when the tip and surface are in the attractive regime).

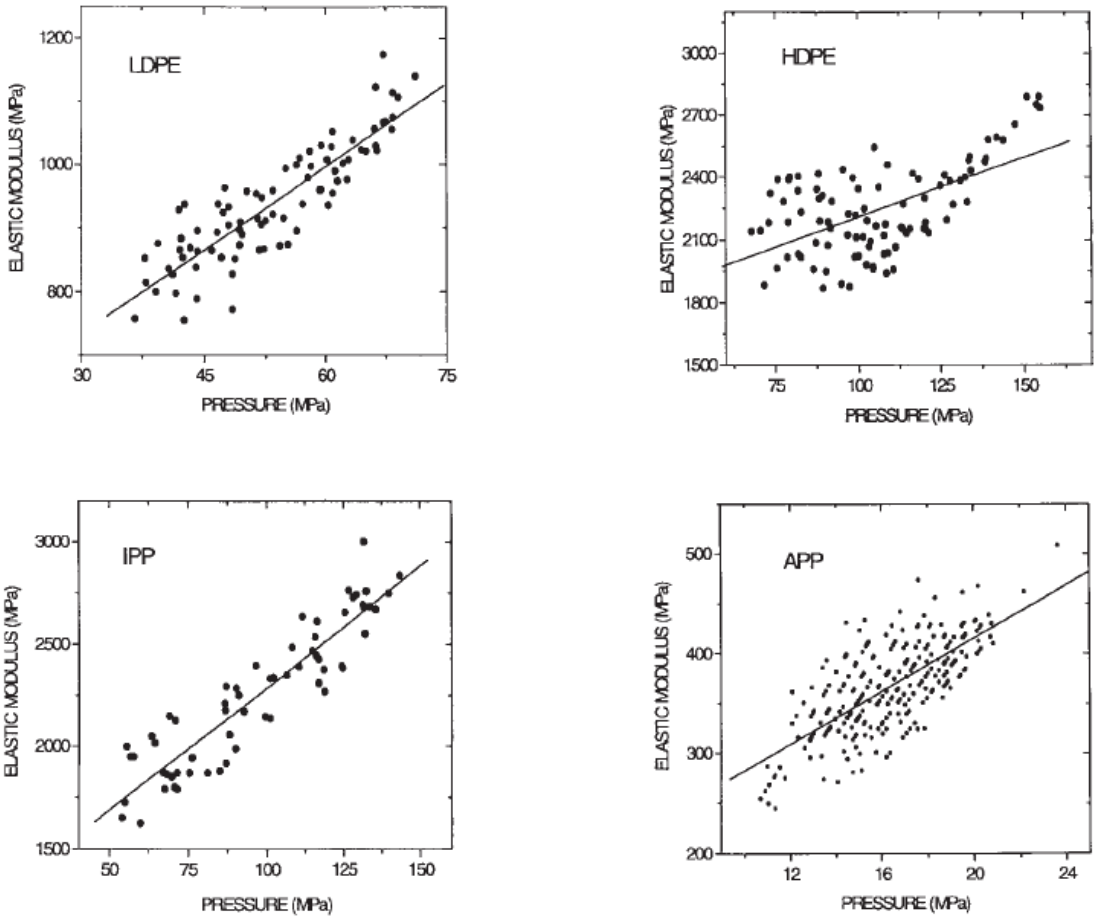

Fig. 6. Pressure versus elastic modulus for LDPE, HDPE, aPP, and iPP.

The friction force can be defined as the product of the shear strength of the polymer (τ) multiplied by the contact area (A).[36] Like the elastic modulus, the shear strength also has a dependence on pressure. From these experiments, an exact dependence of the friction force (F) on the load (W) has been determined (Equation 2)—within the elastic limit, at low pressures. The additional variable, γ, is the surface energy per unit area of the polymer.

$$F = \tau A = \tau\left[\frac{3\pi^{3/2}R(1-\nu)}{4E}\left(W + 3\pi R\gamma + \sqrt{6\pi R\gamma W + (3\pi R\gamma)^2}\right)\right]^{2/3} \quad (2)$$

Friction at different contact pressures/area

The effects of contact pressure are clearly seen when friction force on a polymer is studied with the AFM, MFM, and POD setups described in the instrumental methods section.[23] We have performed friction experiments on LDPE, HDPE, and silicon surfaces with the three instruments using loads and contact areas that vary by approximately eight orders of magnitude. Silicon is a nonpolymeric sample and its microstructure is insensitive to contact pressure variations. It is used as a reference to measure the friction behavior of polymers associated with pressure-induced microstructure changes.

LDPE and HDPE exhibit friction transitions that are pressure controlled and also transitions that are contact area controlled. The pressure-controlled transitions are attributed to transitions from a primarily *elastic* contact between the tip and sample to a *plastic* contact. The contact area transition is attributed to a polymer alignment effect. In contrast to the polymer samples, only pressure-controlled transitions are observed to occur on silicon. A transition from elastic to plastic deformation is seen at contact pressures that are sufficiently high to cause rupture of the native oxide film.

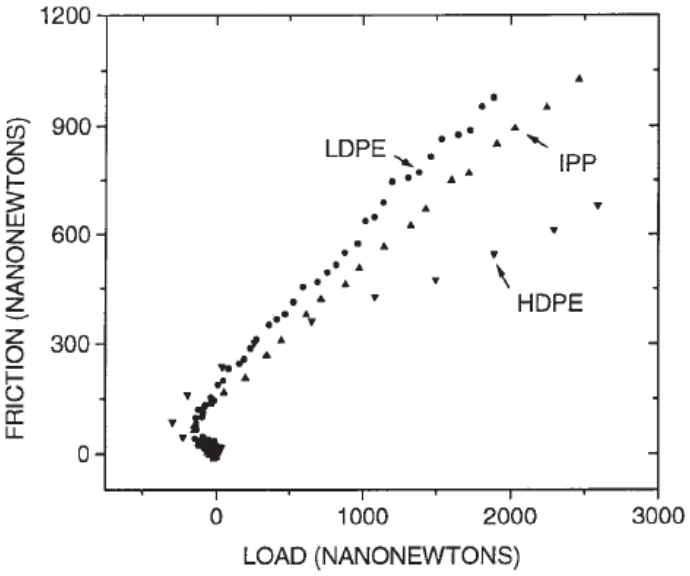

Fig. 7. Friction versus load curves for LDPE, HDPE, and iPP.

Table 2 summarizes the contact areas, pressures, and friction properties collected for LDPE under each set of scanning conditions. The results for HDPE are similar. The AFM yields the lowest friction coefficients. This is attributed to an *elastic deformation* dominated friction process. However, at loads above

Table 2. Friction coefficients and friction behavior of LDPE under different contact pressures and contact areas.

Instrument	Pressure	Contact area	Friction coefficient	Friction mechanism
AFM	25–70 MPa	200–2800 nm^2	0.06	Elastic
AFM	70–105 MPa	2800–6700 nm^2	0.17	Plastic
SFM	42–1625 MPa	1300 nm^2–1.9 μm^2	0.18	Plastic
SFM	8–67 MPa	0.25–15 μm^2	0.13	Elastic
POD	9–16 MPa	1900–5300 μm^2	0.41	Shear alignment

200 n*N*, we observe *wear-dominated* friction and a jump in the friction coefficient. The mean pressure under the AFM tip at 200 n*N* is ~70 MPa for LDPE—higher than the minimum stress required to initiate permanent plastic deformation (~50 MPa).[37]

When the contact pressures are similar, the AFM and the SFM yield similar friction coefficients. However, as the load is increased in the SFM, wear processes dominate and there is a dramatic rise in the friction coefficient. For the POD experiment, the size of contact area becomes an important parameter. The relatively low pressures used in the POD experiment suggest an elastic contact and therefore a low friction coefficient. However, the friction coefficient measured is the highest of all three instruments. This suggests that under large contact areas, the friction process involves an additional mechanism—orienting the polymer in the direction of the scan. Because extra work is necessary to induce this shear alignment, a higher friction coefficient is obtained.

Stretched polymer surfaces

The effect of contact pressure on the friction and wear properties is also seen on the surface of LDPE that is stretched.[38] In this case, indentation and wear experiments show that stretching the polymer decreases the surface yield strength of the polymer, and consequently increases the susceptibility to abrasive (plastic) wear mechanisms. The experimental setup is shown in Figure 8. Briefly, a dumbbell shaped test piece of polyethylene is stretched to a specified strain. After the polymer has relaxed to an equilibrium stress, the texture and mechanical properties are measured.

Indentation tests show that, for the same indentation load, the depth and area of the indent increase when the polymer is stretched (Fig. 8). The most dramatic increase in the depth of the indents is seen when the polymer is stretched near its tensile yield point (~10% elongation). This directly indicates that the *plastic* component of the indentation process has become more important, and shows that the surface yield stress has decreased as a result of the tensile strain (stretching).

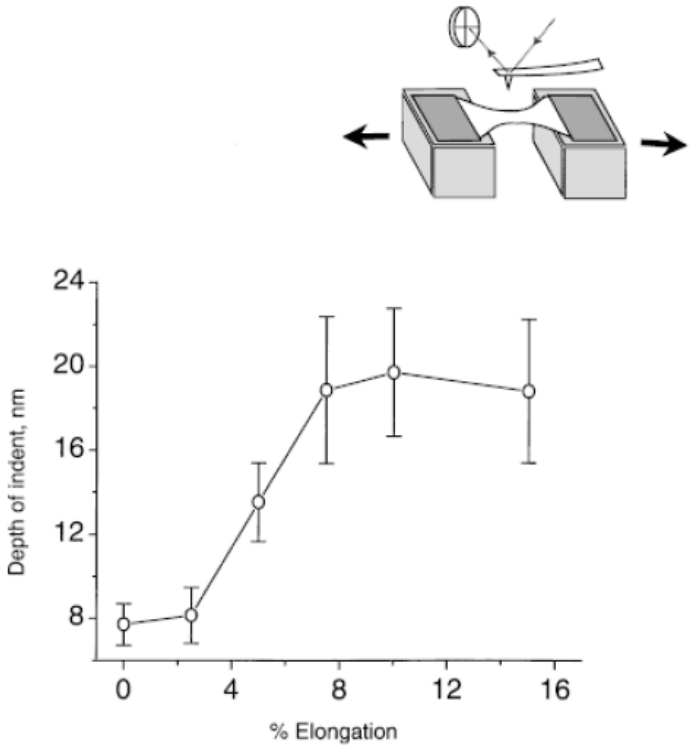

Fig. 8. Depth of indent versus elongation for LDPE. Inset: experimental setup for the stretching experiments.

The lowered yield stress of the surface increases the susceptibility to abrasive wear (plastic wear). A characteristic wear pattern for LDPE is shown in Figure 9(a). When contact pressures high enough to induce permanent plastic damage to the polymer (~50 MPa) are applied, a wear pattern characterized by ridges that run perpendicular to the scanning direction is formed. Under these high pressures the AFM tip presses deep into the polymer and pushes a ridge of material in the direction of the scan [inset of Fig. 9(a)]. Eventually, the tip slides over the ridge and forms a new contact. The depth and spacing of the ridges increases with the load [Fig. 9(b)], indicating that the tip penetrates deeper into the sample at high loads. The depth of the grooves and spacing between the ridges also in-

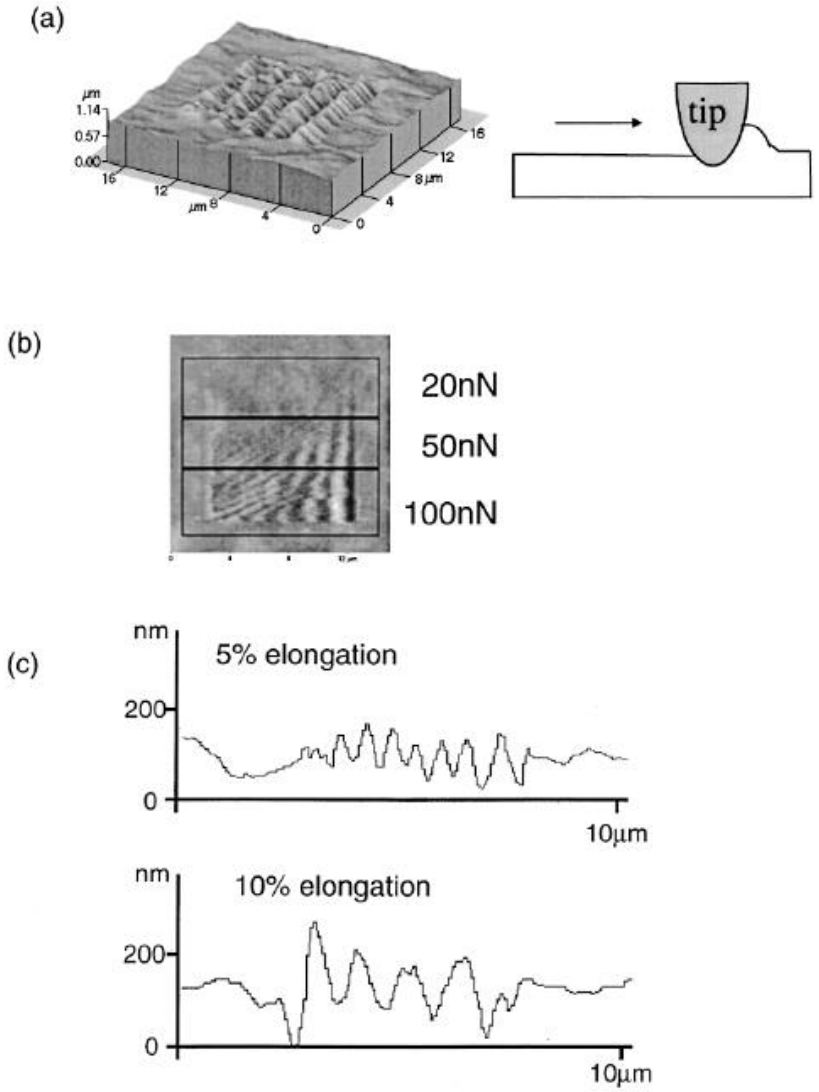

Fig. 9. (a) Characteristic AFM wear pattern on LDPE. Inset: schematic of wear mechanism. (b) Load dependence of the wear pattern. (c) Stretching dependence of the wear pattern.

creases when, for the same load, the polymer is stretched [Fig. 9(c)]. The most dramatic increase in wear is again seen when the polymer is stretched to its tensile yield strain.

In addition to the wear properties, we have used AFM to characterize the microscopic morphology and to probe the surface elasticity of LDPE and HDPE as they are stretched. These surface measurements are interpreted in the context of the bulk stress versus strain curve for polyethylene. Bulk polyethylene contains amorphous and crystalline phases that are mixed together in a random distribution of micron sized spherulitic superstructures. Spherulitic domains are shown in Figure 10. As the polymer is stretched, these domains elongate in the direction of the stretch.

At elongations less than the yield strain, the spherulitic structures at the surface elongate under stress and contract immediately and reversibly when that stress is removed. This causes a reversible roughening effect that can be characterized by the RMS roughness—essentially the variance in height over a given area. Figure 11(a) shows a linear dependence of RMS roughness on elongation.

Stretching beyond the yield strain, the spherulites continue to elongate in the direction of the stress and become narrower perpendicular to the stress. The roughening effect is still linear for both HDPE and LDPE [Fig. 11(b)], but the effect is no longer immediately reversible. When the stress is removed, it takes several minutes for the polymer to relax (contract). As HDPE and LDPE are stretched into the neck propagation zone, the spherulite microstructure breaks down and the polymers are drawn into fibers.

The surface elastic modulus of HDPE as a function of elongation is shown in Figure 11(c). The surface elastic modulus essentially changes as the bulk mechanical properties change. The elastic modulus increases at elongations below the yield strain, suggesting that the deformations at the surface are largely a result of amorphous regions responding elastically to the stress. This is consistent with the elastic modulus measurements made under low pressure, where a linear increase in elastic modulus with pressure is seen. At the tensile yield point, the surface elastic modulus decreases—consistent with the bulk strain softening effect seen on the bulk stress versus strain curve.[38] The strain softening effect is associated with crystalline deformation of the polymer.

The results of these sets of experiments highlight the importance of understanding the mechanical properties under low pressure, high pressure, and stretching conditions. In general, the friction force increases as the load is increased, but a marked increase in the friction is seen when the contact pressure exceeds the stress needed to induce plastic flow (related to the yield strength of the polymer). The stretching experiments indicate that when a polymer is used in an application that subjects the bulk material to complex mechanical stresses (i.e., an artificial hip), the surface mechanical properties continuously change as the nature of the stress changes. The changes in surface properties will have a direct influence on determining the contact area and contact pressure, which will then determine the predominant friction and wear mechanisms of the material.

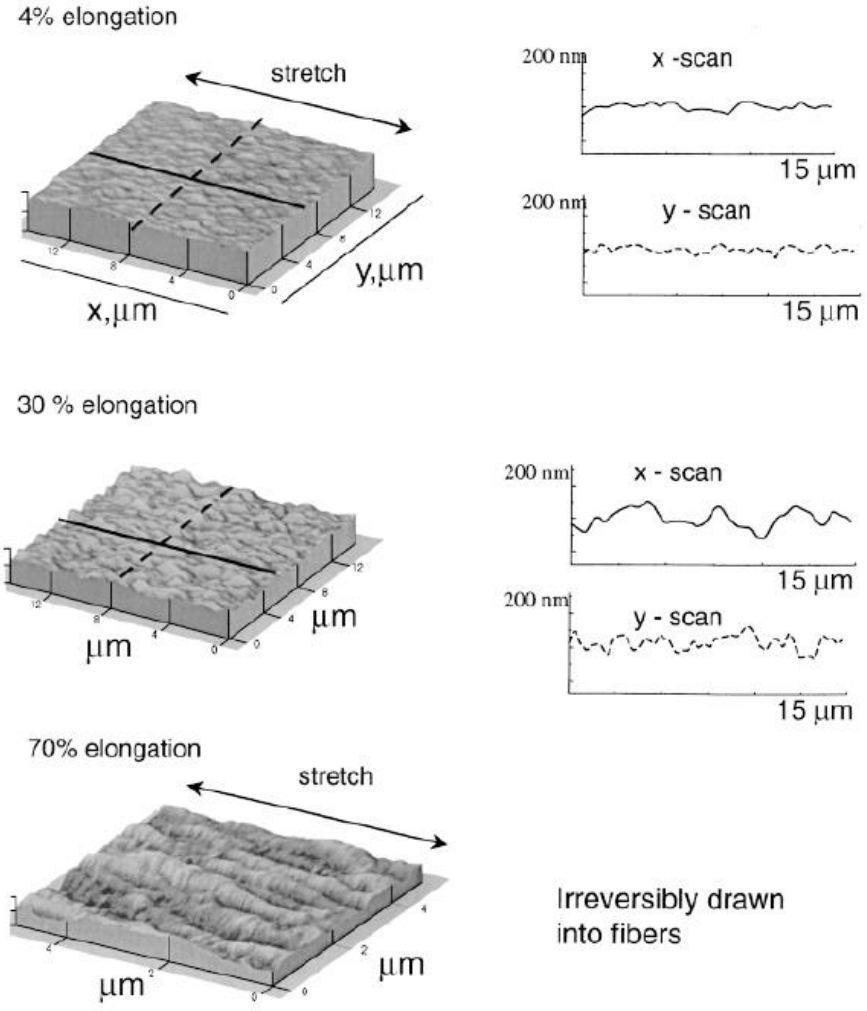

Fig. 10. AFM images of stretched HDPE.

Additionally, we have shown that for polymers that have inhomogeneous microstructure, like polyethylene, bulk mechanical deformation can dramatically change the surface texture. In some applications, this change in surface texture may directly enhance the wear of the material by changing the nature of the contact area at the polymer surface.

Effect of copolymer composition on surface mechanical properties

In addition to polyolefin surfaces, SFM is used to study the surface mechanical properties of additive-free polyurethane consisting of soft segments (SS) made of polyether (PTMO) and hard segments (HS) made of 4,4′-diphenylmethane diisocynatate and 1,4-butanediol (see Fig. 1 for structure).[24] The hard and soft segment distinction is possible because of the large difference in glass temperature of the two components (–40°C for the SS and +50°C for the HS). The bulk mechanical properties of these polyurethane based copolymers can be modified by changing the chemical nature or the relative concentrations of the hard and soft segments.

In contrast to the polyethylene and polypropylene surfaces where crystallinity increases the complexity of the microstructure and affects the mechanical properties, these polyurethane copolymers have a complex structure controlled by hydrogen bonding between the HS and SS. The N-H component of the HS is capable of hydrogen bonding to either the C=O from the HS or to the –O-ether groups from the SS. However, it has been widely observed that the rigid and polar HS tends to interact strongly with other HS and does not mix homogeneously with the less polar SS, creating a microphase separated system.[39]

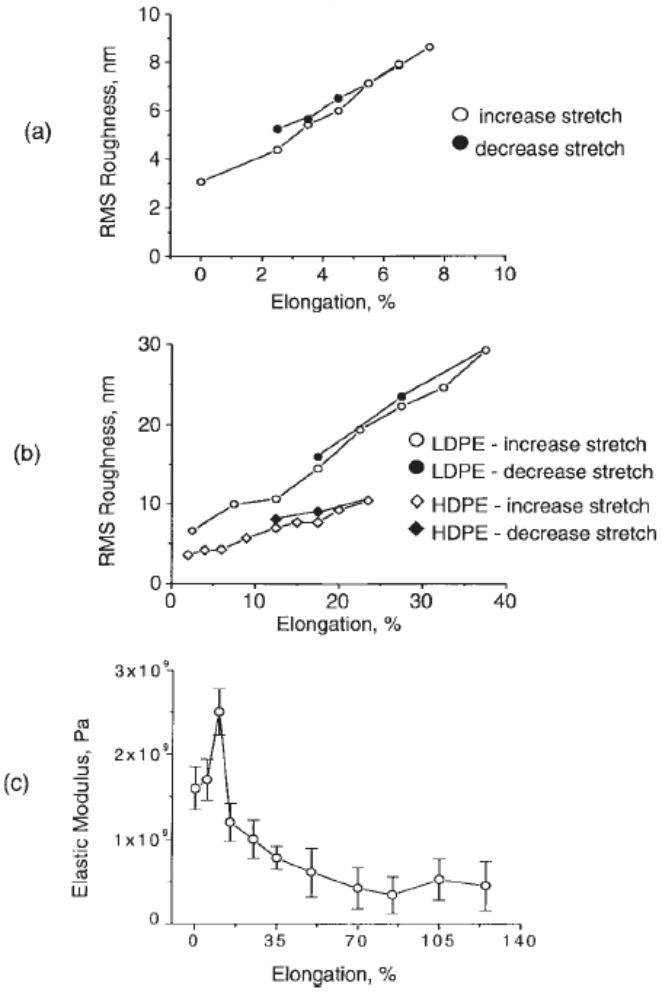

Fig. 11. (a) RMS roughness versus elongation at low elongations (LDPE). (b) RMS roughness versus elongation at intermediate elongations (LDPE and HDPE). (c) Elastic modulus versus elongation (HDPE).

Conventional IR spectroscopy can be used to characterize the degree of microphase separation of HS and SS in the polymer bulk by monitoring the carbonyl stretch at 1700 cm^{-1} (from the HS). When the C=O is hydrogen bonded to the N-H (also from the HS), there is a characteristic blue shift in the carbonyl stretching frequency. Increasing the HS concentration tends to increase the amount of microphase separation and makes the polymer more elastically rigid.

Indentation experiments using the SFM were carried out on the surfaces of copolymers containing 42, 57, 69, and 100% HS in order to determine how bulk microphase separation of the SS and HS leads to different surface properties. Bulk material properties and friction coefficients are summarized in Table 3.

Adhesion was measured as the force required to separate the tip from the sample. Based on the number of polymer units capable of participating in hydrogen bonding, a factor that increases adhesion, one would expect that the 69 and 100% HS samples would have the highest adhesion. However, the strongest pull off force was measured on the 57% HS sample [Fig. 12(a)]. We believe that the low adhesion measured on the 69 and 100% HS samples is attributed to the associative nature of the hard segments; the 57% HS sample has a high adhesion because it has the highest number of nonassociated urethane groups.

The different microstructures of the four samples gives rise to different types of friction mechanisms [Fig. 12(b)]. For the 42% HS sample, which exhibits the lowest microphase separation, the relaxation process of the polymer causes the tip to sink into the sample as it slides across the surface at constant scanning load. This sinking effect gives rise to a large friction coefficient. For the 69% HS sample, the tip rises as it slides across the surface. We believe this effect is caused by a pile-up of material at the leading edge of the contact area. The lowest friction coefficient was obtained on the intermediate HS sample, the 57% sample. In this case, the tip does not sink or rise but remains at a nearly constant depth as it traverses the surface.

Similar to results for the polyethylene surface, polymer deformation is the predominant friction mechanism. Generally, the friction force can be divided into an adhesive component and a deformation component.[21] High adhesive force leads to high friction force. If the adhesive component was the friction controlling component then we would expect that the highest friction forces would be measured on the 57% HS sample (which exhibits the highest adhesion), and that the 42 and 69% HS samples would have lower friction coefficients. Our observation that the 57% HS sample has the lowest friction coefficient suggests that for this set of polymers, the material deformation of the polymer surface controls the surface friction.

Table 3. Bulk material properties and friction coefficients of the polyurethane copolymers.

	42% HS	57% HS	69% HS
M_n	133,213	74,315	76,557
M_w	245,708	109,698	108,508
Elastic modulus (MPa)	21	101	556
Friction coefficient	0.6	0.4	0.9

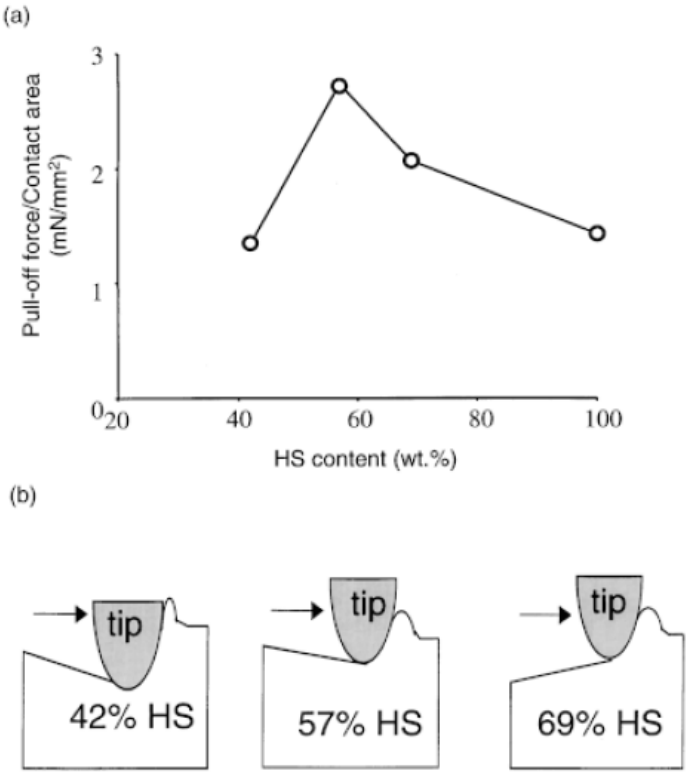

Fig. 12. (a) Adhesive pull off force versus hard segment concentration. (b) Schematic representation of the friction mechanism for the 42, 57, and 69% hard segment copolymers.

Surface Segregation

The surface structure and mechanical properties of a polymer are strongly influenced by crystallinity and microstructure, but can be also be influenced by the segregation of additives or a particular component of the polymer to the surface. We have shown that low molecular weight additives can migrate to the surface and alter the surface mechanical properties of polyethylene.[40] End group segregation is detectable for polymers with end group chemistry that is significantly different than the backbone chemistry.[41] Finally, we show that for miscible polymer blends, simple rules can be used to predict which component will preferentially cover the surface.[11,42,43]

Surface segregation of polymer additives

Low molecular weight additives have been detected at the surface of polyethylene samples by SFG, and have been shown to have a dramatic influence on the surface mechanical properties. In general, commercial polyolefins contain small amounts of stabilizers that can aid in processing and help to prevent oxidation. Typically, these stabilizers are short chain surfactant types of molecules.

We have compared the surface properties of a commercial sample of polyethylene to a pure polyethylene and noticed remarkable differences. Raman spectra for the commercial and pure polyethylene are identical, while SFG spectra for the two polymers are remarkably different (Fig. 13). The SFG spectra of the pure sample shows a strong CH_2 symmetric peak at 2850 cm^{-1} and an antisymmetric peak at 2920 cm^{-1}. The strong peak at 2820 cm^{-1} for the commercial sample indicates that the surface is covered with methoxy groups, a common chemical group of polymer additives.

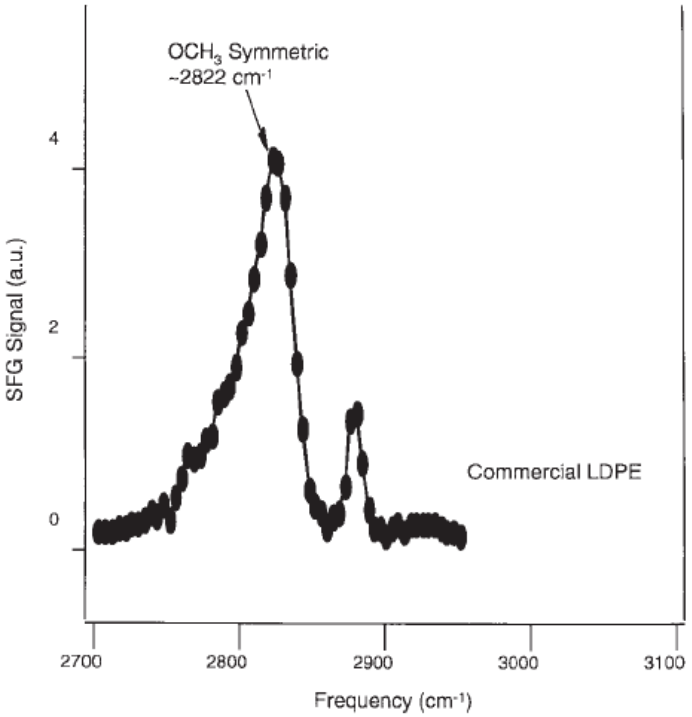

Fig. 13. SFG spectra of commercial LDPE (ssp).

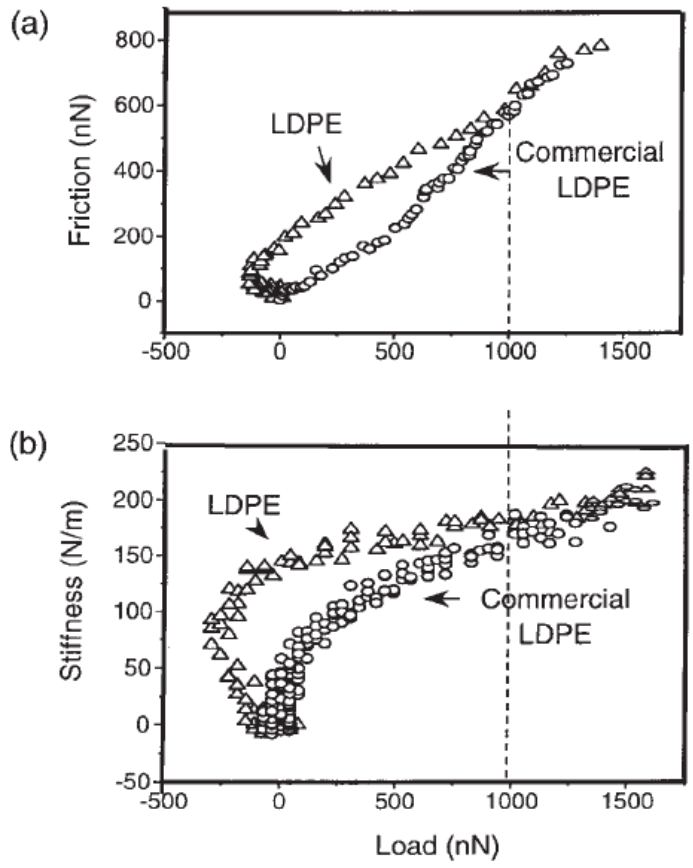

Fig. 14. (a) Friction versus load curves for LDPE and commercial LDPE. (b) Elastic modulus versus pressure for LDPE and commerical LDPE.

We have used AFM to determine how the additive affects the surface mechanical properties. Friction versus load curves for both samples are shown in Figure 14(a). Curves of elastic modulus versus contact pressure are shown in Figure 14(b). The commercial sample exhibits much lower friction at low loads than the laboratory grade sample. At loads above 1000 n*N* (corresponding to a depth of 7–8 nm), however, the friction properties of the two samples are almost identical. Also, the elastic modulus of the commercial sample is much lower than the laboratory grade sample until the load reaches 1000 n*N*. The low friction indicates that the additive lubricates the surface. The low elastic modulus indicates the additives make the surface elastically weaker than the bulk.

Surface segregation of polymer end groups

In addition to low surface energy additives, a great deal of evidence suggests that the end groups of polymer chains can selectively migrate to the polymer surface.[44,45,46] The strongest cases tend to be when the chemical nature of the end group is very different from the backbone (i.e., hydrophobic end groups and hydrophilic backbones). However, end group segregation has also been detected where the energetic difference between the backbone and the end group is minimal.

In our laboratory we have studied the surface structures of PEG with hydrophobic end groups and with hydrophilic end groups (Fig. 1).[41] The different surface tensions between PEG diol (42.9 dyne/cm^2) and PEG methyl ether (37.1 dyne/cm^2) indicate that the hydrophobic end group of the PEG methyl ether affects the surface structure. This difference in surface structures is not detectable by conventional IR techniques, but the different surface structures of PEG, PEG methyl ether, and PEG dimethyl ether can be detected by SFG, as shown in Figure 15. The differences are directly attributed to polymer end group segregation.

The SFG spectrum of PEG diol shows the strong CH_2 symmetric peak of $–OCH_2–$ at 2865 cm^{-1} and does not show an O–H stretch signal in the frequency range from 3000–3800 cm^{-1}. This indicates that the surface is covered by the hydrophobic components of the polymer backbone. The surface spectrum of PEG methyl ether has two strong peaks. The small peak at 2865 cm^{-1} is assigned to the backbone and the stronger peak at 2820 cm^{-1} is assigned to the symmetric stretch of the $–OCH_3$ *end group*. This shows that the more hydrophobic methoxy end groups cover a fraction of the surface and the backbone covers the rest. Again, no hydrophilic hydroxyl end groups can be detected on the surface. The very strong peak at 2820 cm^{-1} for the PEG dimethyl ether film shows that the surface coverage of the hydrophobic $–OCH_3$ end group is even higher for this sample.

Surface segregation in miscible blends

Polymer blends are widely used as a means of tailoring the bulk and the surface properties of materials for various industrial and biomedical purposes. They are of fundamental importance in studying interfacial phenomena of macromolecular systems and of technological interest in applications associated with wetting, adhesion, and tribology. A unique feature of these systems is that the surface composition and structure, and consequently the surface properties of the material, are often different from that of the bulk.[47] This is due to a surface enrichment of the component with the lower surface energy so as to minimize the total surface energy of the system.

To better understand the surface chemistry of polymer blends at a molecular level, we have investigated several two- Again, no hydrophilic hydroxyl end groups can be detected on the surface. The very strong peak at 2820 cm^{-1} for the PEG dimethyl ether film shows that the surface coverage of the hydrophobic $-OCH_3$ end group is even higher for this sample.

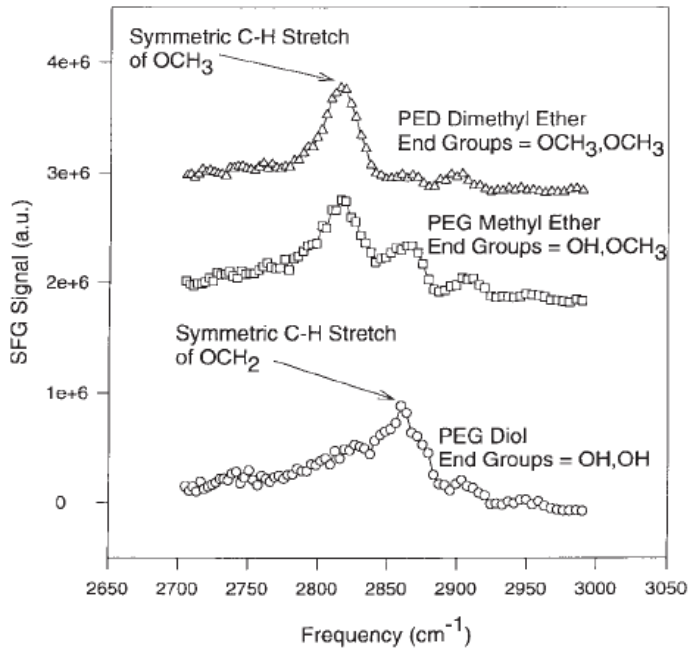

Fig. 15. SFG spectra of PEG, PEG methyl ether, and PEG dimethyl ether (ssp).

Surface segregation in miscible blends

Polymer blends are widely used as a means of tailoring the bulk and the surface properties of materials for various industrial and biomedical purposes. They are of fundamental importance in studying interfacial phenomena of macromolecular systems and of technological interest in applications associated with wetting, adhesion, and tribology. A unique feature of these systems is that the surface composition and structure, and consequently the surface properties of the material, are often different from that of the bulk.[47] This is due to a surface enrichment of the component with the lower surface energy so as to minimize the total surface energy of the system.

To better understand the surface chemistry of polymer blends at a molecular level, we have investigated several two-component polymer blends using a combination of surface techniques: SFG, AFM, and contact angle measurements.[11,42,43] Correlating the surface chemical composition (by SFG), the surface structure (by AFM), and the surface free energy (by contact angle goniometry),[48] we can provide a molecular understanding of the surface chemistry of polymer blends.

The two component polymer blends are the Biospan-S/phenoxy base polymer blend (BS/PHE), the Biospan-SP/phenoxy base polymer blend (BSP/PHE), and the Biospan-F/phenoxy base polymer blend (BF/PHE). The molecular structures of these four polymers are shown in Figure 1.

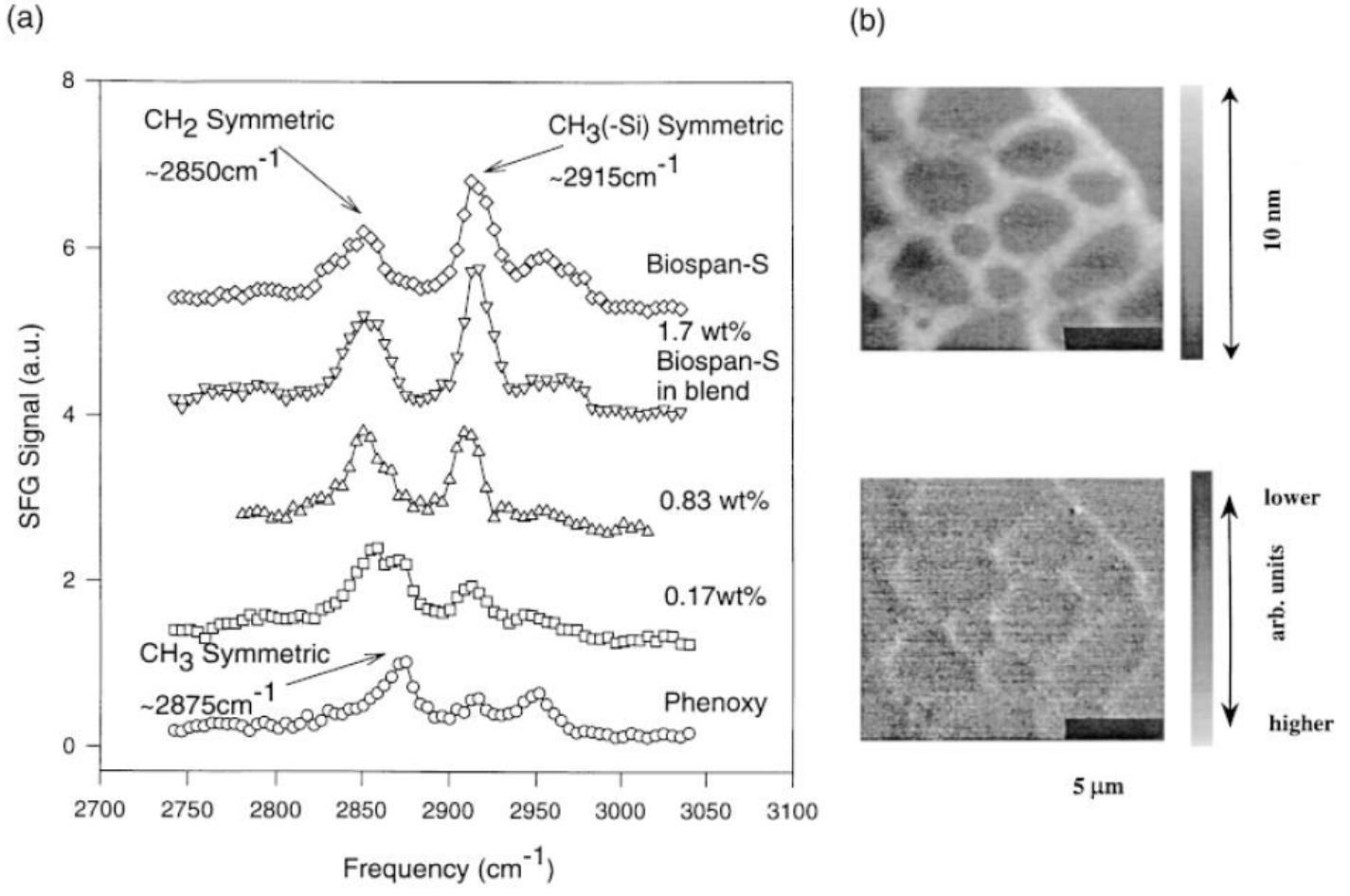

Fig. 16. (a) SFG spectra of BS/PHE blends (ssp). (b) AFM topography and friction image of BS/PHE blend showing intermediate coverage.

Biospan-S is a polyurethane capped with poly(dimethylsiloxane) (PDMS) end groups. Biospan-SP is similar to BS but 30% of the PTMO in the BS backbone is replaced by poly(ethylene oxide) (PEO). Biospan-F is composed of the same polyurethane as BS except the polyurethane is capped by fluorinated (–(–CF_2–)n–) end groups.

Miscible blends of a phenoxy polymer with a block or segmented copolymer produce extrudable and moldable compounds that soften at a glass transition temperature determined by the wt % composition of the blend—generally between room temperature and body temperature. These polymer blends are ideal candidates for various biopolymer applications, such as intravenous catheter tubing that will soften after insertion into a vein.

SFG spectra for BS, PHE, and BS/PHE blends are shown in Figure 16(a). These spectra show that the BS component segregates at the polymer blend surface and approaches a maximum BS surface coverage when its bulk concentration is only 1.7 wt %. When the BS concentration is lower than 0.17 wt %, the polymer surface is dominated by the PHE base polymer. In the intermediate BS concentration region, 0.17– 1.7%, the relative BS surface content increases in a stepwise manner with the addition of BS. These findings correlate well with contact angle results, which show that the surface free energy decreases in the same way as the SFG determined surface ratio of PHE to BS.[43]

AFM images show that when the BS bulk concentration is in the intermediate surface coverage regime (0.17–1.7 wt %), there is a segregation of each component, BS and PHE, to form a domain structure at the polymer surface. The domains [Fig. 16(b)] are distinguishable by the friction properties of the two components—the PHE component exhibits twice the friction of the BS component at a load of 20 n*N*. Therefore, AFM images of the frictional force allow one to differentiate between the two components on the surface. Below 0.17 wt % of BS, the friction and morphology of the polymer blend surface is very similar to that of pure PHE; while above 1.7 wt %, the morphology of the blend surface resembles that of pure BS.

This set of results clearly shows that surface enrichment of the low surface-energy component lowers the total surface energy of the polymer blend. The stepwise variation of the surface chemistry found in this polymer blend shows a viable way to precisely control the polymer surface properties through the bulk composition of the blend.

Figure 17(a) and (b) show spectra for the BSP/PHE and BF/PHE blends. For the BSP/PHE blend, spectra show that the surface is fully covered by PHE when the BSP concentration is below 0.25 wt %, and the surface is covered completely by BSP at bulk concentrations of 3.5 wt % and higher.

The differences between BS/PHE and BSP/PHE demonstrate that BSP is not as surface-active as BS. This can be explained by the higher surface tension of BSP (26 dyne/cm^2) compared to BS (22 dyne/cm^2). The higher surface tension comes from the replacement of 30% PTMO in BS with PEO, a more hydrophilic polymer. This makes BSP less surface-active than BS.

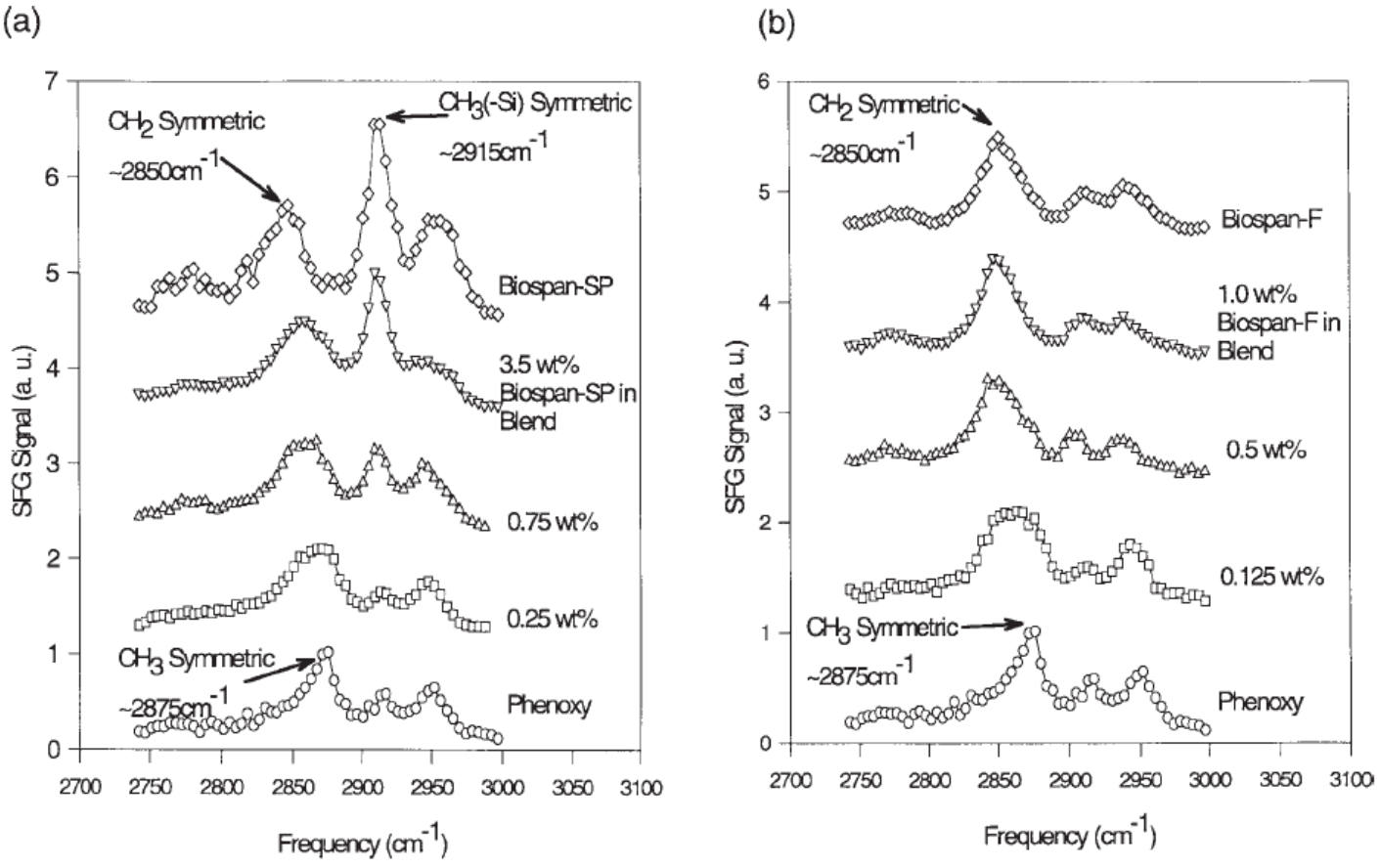

Fig. 17. (a) SFG spectra of BS/PHE blends (ssp). (b)SFG spectra of BF/PHE blends (ssp).

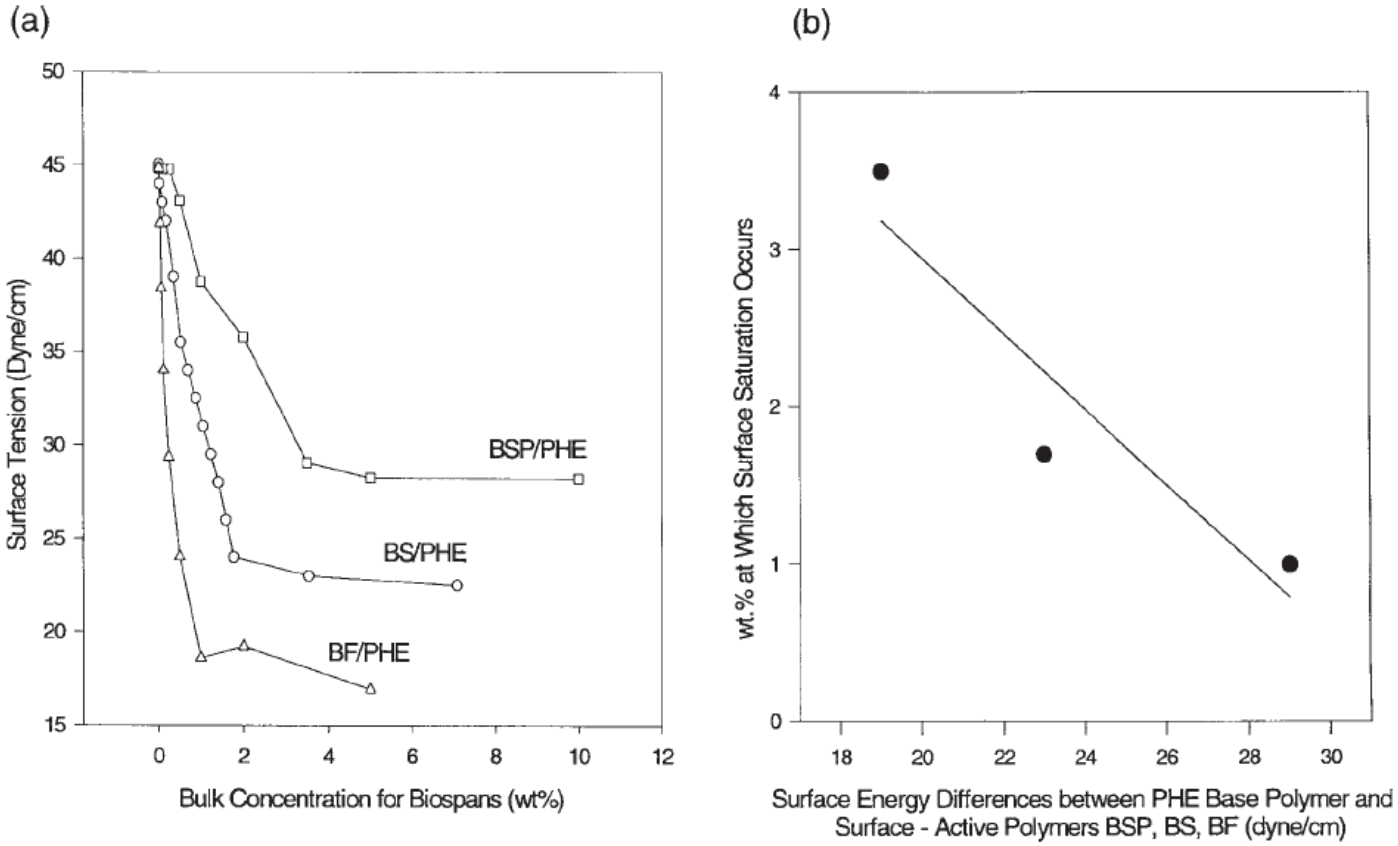

Fig. 18. (a) Surface tension as a function of blend composition. (b) Correlaton between minimum bulk concentration and surface energy difference.

This set of results clearly shows that surface enrichment of the low surface-energy component lowers the total surface energy of the polymer blend. The stepwise variation of the surface chemistry found in this polymer blend shows a viable way to precisely control the polymer surface properties through the bulk composition of the blend.

Figure 17(a) and (b) show spectra for the BSP/PHE and BF/PHE blends. For the BSP/PHE blend, spectra show that the surface is fully covered by PHE when the BSP concentration is below 0.25 wt %, and the surface is covered completely by BSP at bulk concentrations of 3.5 wt % and higher.

The differences between BS/PHE and BSP/PHE demonstrate that BSP is not as surface-active as BS. This can be explained by the higher surface tension of BSP (26 dyne/cm^2) compared to BS (22 dyne/cm^2). The higher surface tension comes from the replacement of 30% PTMO in BS with PEO, a more hydrophilic polymer. This makes BSP less surface-active than BS.

The BF surface has the lowest surface tension (16 dyn/cm^2) and is the most surface-active. This is seen in a comparison between polymer blends BF/PHE and BS/PHE. The BF component begins to appear on the BF/PHE blend surface when its bulk concentration is only 0.031 wt %, and it fully covers the surface when the concentration is 1 wt %.

The surface tensions of the three polymer blends as a function of blend concentration are presented in Figure 18(a). The curves show that the lower the surface energy of the surface-active polymer (surface tension: BF < BS < BSP), the easier it is for it to saturate the polymer blend surface [minimum bulk concentration for surface saturation: BF (1 wt %) < BS (1.7 wt %) < BSP (3.5 wt %)].

Figure 18(b) describes the correlation between these minimum bulk concentrations and the surface free energy differences of the PHE base polymer and the three surface-active polymer components, BF, BS, and BSP. Surface activity increases as the difference in surface tension between the base polymer (solvent) and the surface-active additive polymer (surfactant) increases. This relationship may be used to predict the wt % of other surface-active polymers that would be required to mix into PHE and fully cover the surface of the polymer blend.

Surface restructuring of polymer blend surfaces in water

Because BS, BSP, and BF contain both hydrophobic [PDMS or (–(–CF_2–)n–)] and hydrophilic (ether and urethane segments) components, their surface structures may be expected to differ in water and in air. SFG spectra of the polymer blends after exposure to water show that the surfaces of the blends are environmentally sensitive. The degree of restructuring, however, depends on the relative surface energies of the two components.

When a 3.5 wt % BSP/PHE blend polymer is in contact with water for 1 week, the surface is still dominated by BSP (Fig. 19). However, the surface concentration of the BSP end groups (PDMS) does decrease—the surface is now covered more by the hydrophilic polyurethane backbone of the BSP. The effect is similar to that seen for the BS/PHE blend exposed to water.[49] In this case, the interaction of water with the polymers is unable to overcome the diffusion barrier for the more hydrophilic PHE to emerge to the surface. The interaction is strong enough, however, for the BSP to rearrange at the surface.

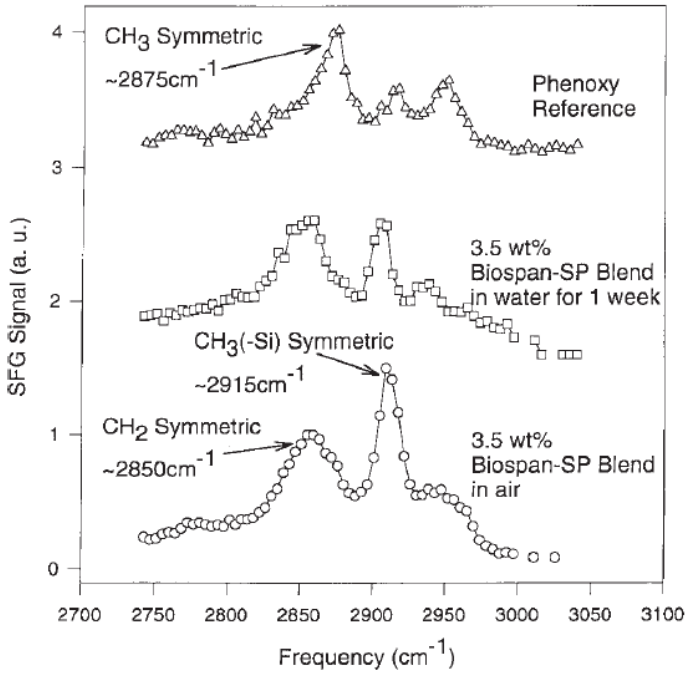

Fig. 19. SFG spectra of BSP/PHE with 3.5 wt % BSP bulk concentration in air and in contact with water (ssp).

When a 1 wt % BF/PHE is placed in contact with water for 5 days, the characteristic peak of PHE at ~2875 cm^{-1} becomes visible [Fig. 20(a)], indicating that for this blend the PHE component emerges to the surface. After drying this BF/PHE blend, the PHE returns the bulk and the BF covers the surface again. The different responses of the 1 wt % BF/PHE and the 3.5 wt % BSP/PHE polymer blends to the environmental change from air to water are because BF is more hydrophobic than BSP, and the wt % of BF in the blend (1%) is lower than BSP (3.5%).

Figure 20(b) shows that for the 5 wt % BF/PHE blend, the surface is dominated by BF in both air and water. This is probably because the BF layers on the 5 wt % BF/PHE surface are thicker than those on the 1 wt % BF/PHE surface, inhibiting migration of PHE to the surface.

Conclusion

Polymers remain free of contamination by adsorbed gases, as compared to the much more chemically sensitive metals and oxides. In many cases this makes it possible to carry out molecular scale investigations of their surface properties without the need of vacuum. SFG surface vibrational spectroscopy and AFM have been used in our laboratory to study the surface structure and mechanical properties (friction, wear, elastic modulus, and hardness) of polymer surfaces.

Polyethylene and polypropylenes were the focus of some of these studies. Contact pressure and contact area were shown to be important parameters in determining the friction properties of the polymers. Stretching of polymers was shown to lead to surface roughening and alteration of surface mechanical properties. Polyurethane copolymers and polymer chains with variable hydrophilic or hydrophobic end groups were the focus of other studies. Polyurethane copolymers show complex changes in their surface mechanical properties because of the importance of hydrogen bonding between hard and soft segments. Hydrophobic parts of the polymer chain segregate to the surface in air, while hydrophilic parts surface-segregate in water. Polymers are the steel of the 21st century. The human body is built of biopolymers and manmade polymers are used increasingly as bioimplants. For these reasons, a continued rapid growth of polymer surface science is expected for the future.

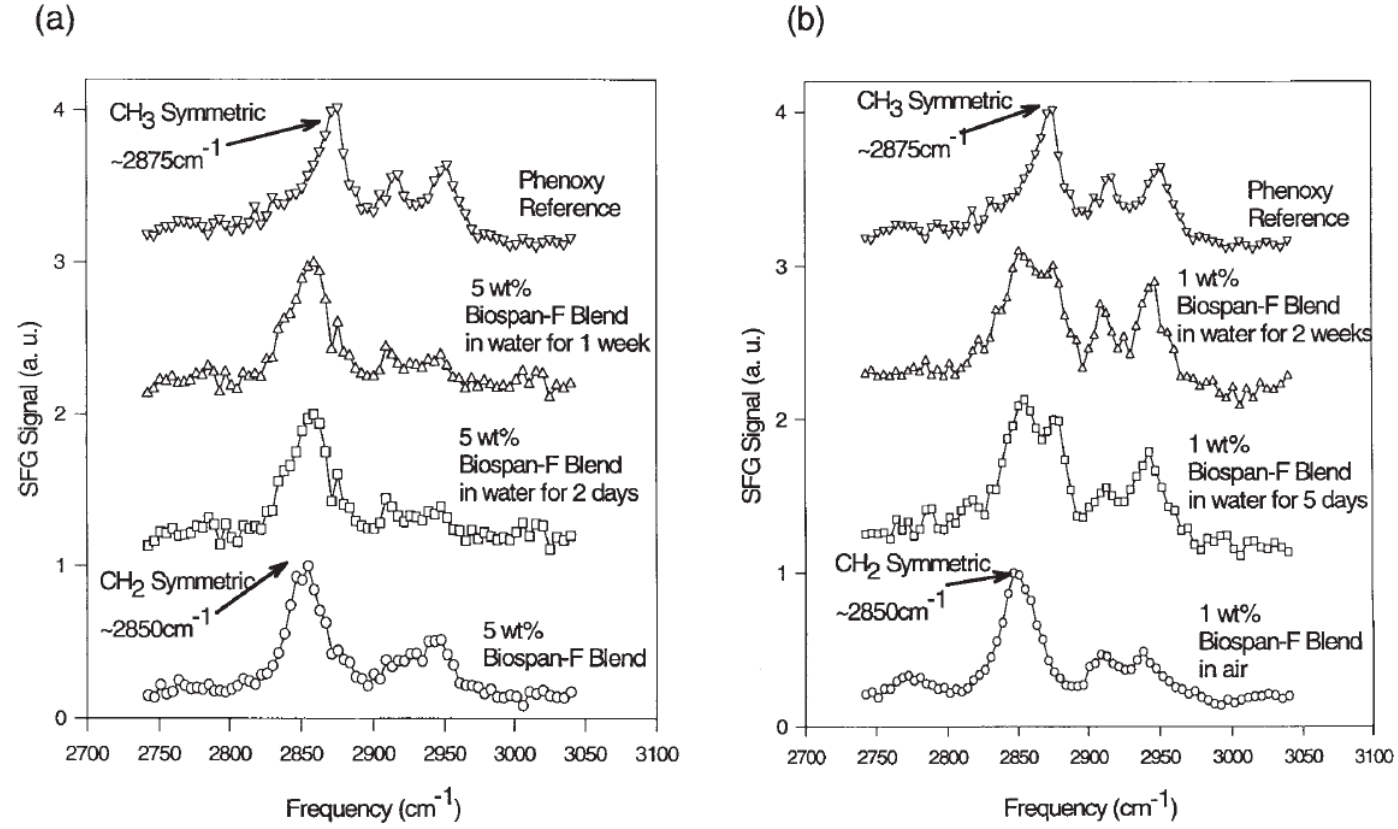

Fig. 20. (a) SFG of BF/PHE with 5% BF bulk concentration in air and in contact with water for 5 days (ssp).
(b) SFG of BF/PHE with 1% BF bulk concentration in air and in contact with water for 5 days (ssp).

REFERENCES

[1] Somorjai, G.A. Introduction to Surface Chemistry and Catalysis; Wiley: New York, 1994.
[2] Shen, Y.R. Principles of Nonlinear Optics; Wiley: New York, 1984.
[3] Hirose, C.; Akamatsu, N.; Domen, K. J Chem Phys 1992, 96, 997.
[4] Hirose, C.; Akamatsu, N.; Domen, K. J Phys Chem 1993, 97, 10064.
[5] Somorjai, G.A.; Su, X.C.; McCrea, K.R.; Rider, K.B. Top Catalysis 1999, 8, 23.
[6] Somorjai, G.A.; Rupprechter, G. J Phys Chem B 1999, 103, 1623.
[7] Shultz, M.J.; Schnitzer, C.; Simonelli, D.; Baldelli, S. Int Rev Phys Chem 2000, 19, 123.
[8] Baldelli, S.; Markovic, N.; Ross, P.; Shen, Y.R.; Somorjai, G.A. J Phys Chem B 1999, 103, 8920.
[9] Wei, X.; Zhuang, X.W.; Hong, S.C.; Goto, T.; Shen, Y.R. Phys Rev Lett 1999, 82, 4256.
[10] Zhang, D.; Shen, Y.R.; Somorjai, G.A. Chem Phys Lett 1997, 281, 394.
[11] Zhang, D.; Gracias, D.H.; Ward, R.; Gauckler, M.; Tian, Y.; Shen, Y.R.; Somorjai, G.A. J Phys Chem B 1998, 102, 6225.
[12] Zhang, D.; Dougal, S.M.; Yeganeh, M.S. Langmuir 2000, 16, 4528.
[13] Shen, Y.R. Appl Phys B 1999, 68, 295.
[14] Wei, X.; Hong, S.C.; Lovosky, A.I.; Held, H.; Shen, Y.R. J Phys Chem B 2000, 104, 3349.
[15] Simpson, G.J.; Rowlen, K.L. J Phys Chem B 1999, 103, 1525.
[16] Simpson, G.J.; Rowlen, K.L. J Phys Chem B 1999, 103, 3800.
[17] Rugar, D.; Mamin, H.J.; Guethner, P. Appl Phys Lett 1989, 55, 2588.
[18] Frohn, J.; Wold, J.F.; Besocke, K.; Teske, M. Rev Sci Instrum 1989, 60, 1200.
[19] Lu, W.; Komvopoulos, K. J Appl Phys 1999, 85, 2642.
[20] Komvopoulos, K.; Saka, N.; Suh, N.P. J Tribol 1986, 107, 452.
[21] Gracias, D.H.; Somorjai, G.A. Macromolecules 1998, 31, 1269.
[22] Burnham, N.A.; Colton, R.J.; Polluck, H.M. Nanotechnology 1993, 4, 64.
[23] Niederberger, S.; Gracias, D.H.; Komvopoulos, K.; Somorjai, G.A. J Appl Phys 2000, 87, 3143.
[24] Mailhot, B.; Komvopoulos, K.; Ward, B.; Tian, Y.; Somorjai, G.A. J Appl Phys (accepted).
[25] Snyder, R.G.; Strauss, H.L.; Elliger, C.A. J Phys Chem 1982, 86, 5145.
[26] Hostetler, M.J.; Stokes, J.J.; Murray, R.W. Langmuir 1996, 12, 3604.
[27] Clark, E.S. In Physical Properties of Polymers; Mark, J.E., Ed.; AIP: New York, 1996, 409–416.
[28] Plazek, D.J.; Ngai, K.L. In Physical Properties of Polymers; Mark, J.E., Ed.; AIP: New York, 1996, 139–160.
[29] Hammerschmidt, J.A.; Gladfelter, W.L.; Haugstad, G. Macromolecules 1999, 32, 3360.
[30] Dinelli, F.; Buenvinje, C.; Overney, R.M. J Chem Phys 2000, 113, 2043.
[31] Tsui, O.K.C.; Wang, X.P.; Ho, J.Y.L.; Ng, T.K.; Wiao, X. Langmuir 2000, 20, 4198.
[32] Gracias, D.H.; Zhang, D.; Lianos, L.; Ibach, W.; Shen, Y.R.; Somorjai, G.A. Chem Phys 1999, 245, 277.
[33] Brooks, N.W.J.; Unwin, A.P.; Duckett, R.A.; Ward, I.M. J Macromol Sci Phys 1995, 34, 29.
[34] Mark, J.E. Physical Properties of Polymers, 2nd ed.; ACS: 1993.
[35] Johnson, K.L. Contact Mechanics; Cambridge University Press: New York, 1987.
[36] Carpick, R.W.; Agrait, N.; Ogletree, D.F.; Salmeron, M. Langmuir 1996, 12, 3334.
[37] Minimum mean pressure required to initiate plastic flow roughly estimated from the Tresca criteria: ~1.6 × (Bulk Tensile Yield Stress). See Reference 35 for a complete description. Minimum mean pressure required to generate *permanent plastic damage* ~4.5 × (Bulk Tensile Yield Stress) from Lemoine, P.; McLaughlin, J. Thin Solid Films 1999, 339, 258.
[38] Opdahl, A.; Somorjai, G.A. J Polym Sci Part B: Polym Phys (submitted).
[39] Samuels, S.L.; Wilkes, G.L. J Polym Sci, Symp No. 43 1973, 149.
[40] Gracias, D.H.; Zhang, D.; Shen, Y.R.; Somorjai, G.A. Tribology Lett 1998, 4, 231.
[41] Chen, Z.; Baldelli, S.; Opdahl, A.; Ward, R.; Shen, Y.R.; Somorjai, G.A. J Am Chem Soc 2000, 122, 10615.
[42] Zhang, D.; Ward, R.S.; Shen, Y.R.; Somorjai, G.A. J Phys Chem 1997, 101, 9060.
[43] Chen, Z.; Ward, R.; Tian, Y.; Eppler, A.S.; Shen, Y.R.; Somorjai, G.A. J Phys Chem B 1999, 103, 2935.
[44] Dee, G.T.; Sauer, B.B. Adv Phys 1998, 47, 161.
[45] Schaub, T.F.; Kellogg, G.J.; Mayes, A.M.; Kulasekere, R.; Ankner, J.F.; Kaiser, H. Macromolecules 1996, 29, 3982.
[46] Zhao, W.; Zhao, X.; Rafailovich, M.H.; Sokolov, J.; Composto, R.J.; Smith, S.D.; Satkowski, M.; Russell, T.P.; Dozier, W.D.; Mansfield, T. Macromolecules 1993, 26, 561.
[47] White, K.A.; Ward, R.S.; Gill, R.S.; Lim, F.; Coviello, S.C. In Surface Modification of Polymeric Biomaterials; Ratner, B.D.; Castner, D.G., Eds.; Plenum Press: New York, 1996.
[48] Fowkes, F.M. Contact Angle, Wettability, and Adhesion, Advances in Chemistry Series 43; ACS: Washington DC, 1964.
[49] Zhang, D.; Ward, R.; Shen, Y.R.; Somorjai, G.A. J Phys Chem 1997, 101, 9060.